

Forecasting seeing for the Maunakea Observatories

Ryan Lyman,¹ Tiziana Cherubini²^{*} and Steven Businger²

¹Maunakea Observatory, 640 North A'ohoku Place, No. 209, Hilo, HI 96720, USA

²Department of Atmospheric Sciences, University of Hawaii, 2525 Correa Road, HIG 350, Honolulu, HI 96822, USA

Accepted 2020 June 14. Received 2020 June 5; in original form 2020 January 13

ABSTRACT

Optical turbulence greatly impacts the range and quality of astronomical observations. Advanced knowledge of the expected atmospheric optical turbulence provides important guidance that helps astronomers decide which instrument to schedule and enables them to optimize the adaptive optics technology that improves image resolution. Along with forecasts of weather conditions, prediction of the optical observing quality on the Maunakea summit has been a goal for the Maunakea Weather Center (MKWC) since its inception more than 20 yr ago. Forecasting optical turbulence, and its derivative, ‘seeing’, has proven to be quite challenging because optical turbulence is too small and complex to directly capture with a regional weather model. Fortunately, the permanent installation of a Differential Image Motion Monitor (DIMM) and Multi-Aperture Scintillation Sensor (MASS) at the summit of Maunakea has made seeing observations available during the last decade, providing valuable feedback to the MKWC. This paper summarizes the experience at MKWC in anticipating optical turbulence for the summit of Maunakea accrued through years of daily operational forecasting, and continuous comparison between MKWC official forecasts, model guidance, and observational measures of seeing. Access to a decade seeing observations has allowed quantification the factors that impact seeing, including wind shear, atmospheric stability patterns, and optical turbulence, and to document the seasonal and intra-seasonal variations in seeing. Consequently, the combination of experience gained, and custom model guidance has led to more accurate seeing forecasts (rms errors averaging <0.25 arcsec since 2012) for the Maunakea astronomical observatories.

Key words: turbulence – atmospheric effects – methods: data analysis – methods: observational – methods: statistical – telescopes.

1 INTRODUCTION

Ground-based astronomy is very dependent upon the whims of the weather and observing conditions. The favourable atmospheric conditions for astronomical observing at Maunakea are well documented. For the most part, the Maunakea Observatories benefit from a very persistent trade wind inversion maintained by a quasi-stationary subtropical ridge to the northeast of the State, which allows predominately dry conditions to prevail at the summit, free of low-level clouds and pollutants for about 70 per cent of the year. In addition, winds travelling over open ocean surrounding Hawaii are undisturbed by upstream orography. The boundary layer over the summit of Mauna Kea under stable conditions at night is rather thin, on the order of 100-m thick. This layer is also known as the ‘surface layer’ or ‘ground layer’ and is the result of a combination of radiational cooling and mechanical mixing by the wind (Businger 1973). The atmosphere above the ground layer, where the direct impact of the surface is no longer felt, is referred to as the ‘free’ atmosphere.

While clement and clear weather is the minimum requirement for the astronomers to be able to conduct their observations, the optical

turbulent state of the atmosphere is also a primary concern because turbulence directly impacts the range of possible observations and ultimate resolving power of the telescopes (Businger & Cherubini 2011). Small-scale temperature and moisture fluctuations associated with turbulence in the atmosphere result in fluctuations of the refractive index (Roddier 1981). The wave front of radiation travelling through the atmosphere changes as it encounters inhomogeneities in the refractive index, degrading optical image quality. The intensity of the turbulent fluctuations of the atmospheric refractive index is described by the refractive index structure function, C_n^2 . The maximum telescope resolution is defined by a parameter called ‘seeing’, that is the full width at the half-maximum of the long-exposure seeing-limited point spread function of a star image at the focus of a large diameter telescope (Coulman 1985; Tokovinin 2002). Seeing is a function of the integral of C_n^2 over the light’s propagation path and is measured in arcseconds.

There has been considerable progress in recent years to observe and quantify the effects of atmospheric turbulence and refractivity gradients on telescope image. Sites characterization studies (Schök et al. 2009; Skidmore et al. 2009; Vernin et al. 2011) have provided good observational data sets. At the same time, there has been progress in modelling these atmospheric effects to support advances in methods that mitigate resulting telescope image degradation: Bougeault et al. (1995), Masciadri, Vernin & Bougeault (1999), Masciadri and

* E-mail: tiziana@hawaii.edu

Jabouille, (2001), Masciadri, Avila & Sánchez (2004), Trinquet & Vernin (2009), and Giordano et al. (2013). In Businger & Cherubini (2011) contributions from experts in the various facets of the complex challenge posed by atmospheric turbulence on optical and longer wavelengths are collected and presented. More recently, Masciadri, Lascaux & Fini (2013) presented a feasibility study to provide operational forecasts of both weather and optical turbulence at the European Southern Observatory. Alternative approaches include the use of autoregression (Kornilov 2016) and machine learning (Milli et al. 2019) techniques.

Recent advances in telescope infrastructure include the innovation of queue scheduling and use of adaptive optics systems (Amico, Campbell & Christou 2010), which allow the best astronomical instrument to be selected for the anticipated atmospheric conditions and mitigation of optical turbulence effects on telescope observations, respectively. Therefore, advanced knowledge of the expected atmospheric optical turbulence and seeing provides important guidance that helps astronomers decide which instrument to schedule and enables them to optimize the adaptive optics technology that improves image resolution.

Advances in high-resolution numerical weather predictions provide the accurate forecasts needed for queue scheduling. Recognition of this match in the late 1990s led to the establishment of the Maunakea Weather Center (MKWC, <http://mkwc.ifa.hawaii.edu>; Businger et al. 2001) at the University of Hawaii at Manoa. Since then the MKWC has provided weather forecasts to help mitigate bad/hazardous weather conditions that impact the summit including: high winds, clouds, rain and snow, and a twice daily weather bulletin. These products are available on the MKWC web pages in time for daily scheduling of nightly astronomical activities. Shortly after its inception, a new goal of the MKWC was to estimate the optical turbulence state of the atmosphere and create a seeing forecast product.

The MKWC locally runs the Weather and Research Forecasting system (WRF, <http://www.wrf-model.org>), a regional numerical weather prediction model, customized for the Maunakea summit and the astronomer’s needs. A C_n^2 /seeing algorithm was developed and implemented within the WRF modelling system and provides guidance to forecasters (Cherubini et al. 2008a; Cherubini, Businger & Lyman 2008b). The algorithm is continuously being refined, calibrated, and updated (Cherubini & Businger 2011, 2013). Recent progress in the development of the algorithm is a topic for a future paper. Despite advances in atmospheric modelling, forecasting optical turbulence and its derivative, seeing, remains a great challenge, because optical turbulence is too small and complex to directly capture with a regional weather model. Fortunately, the permanent installation of a Differential Image Motion Monitor (DIMM) and Multi-Aperture Scintillation Sensor (MASS) at the summit of Maunakea during 2009 September have provided a decade-long time-series of turbulence data that has proven an invaluable resource for understanding seeing and for validation of forecasts and model output at the MKWC. Real time access to these observations has allowed for a greater understanding of the factors that affect seeing, including correlations between wind shear, atmospheric stability, and optical turbulence. The long-running data set allows researchers to investigate the seasonal and intraseasonal variations in seeing. Consequently, the combination of experience gained and custom model guidance has led to increasingly accurate seeing forecasts (rms errors averaging <0.25 arcsec since 2012) for the Maunakea astronomical observatories.

This paper summarizes the experience at the MKWC in anticipating optical turbulence for the summit of Maunakea accrued through years of daily forecasting, and continuous comparison between MKWC official forecasts, model guidance, and observational measures of seeing. The paper describes the relationships found between measured turbulence and larger scale meteorological features observed while forecasting. These relationships are deduced during the everyday process of issuing the weather forecast and by case studies of: (1) model analyses and forecasts available via the NCEP/Global Forecasting System (GFS) and MKWC WRF; and (2) local and remote (satellite) observations of the status of the atmosphere. The daily MKWC seeing forecast is brought to life by a mixture of forecaster’s intuition, experience, and custom model guidance. While forecaster intuition remains a ‘magic ingredient’ that is hard to translate, the understanding gained with MKWC experience can be explained, which is the subject of the remainder of this paper.

2 OPTICAL TURBULENCE MEASUREMENTS

The physical design and performance of the combined MASS and DIMM (MD hereafter) is described in detail in Kornilov et al. (2007). This instrumentation was donated to the Maunakea Observatories by the Thirty Meter Telescope (TMT) project, following their site characterization campaign (Schöck et al. 2009, see <https://www.tmt.org>). Since then the Maunakea Observatories have sponsored the MD’s repair, maintenance, and upgrades. The MD is situated at the top of the Canada–France–Hawaii Telescope (CFHT) instrument tower, approximately 7 m above the ground (Fig. 1). The MD is located between the Gemini and CFHT observatories, and generally unaffected by terrain or other observatories when winds are from the west and east, which occurs 75 per cent of the year (Da Silva 2012). The MD sampling frequency is about 90 s.

DIMM measures the integrated optical turbulence through the entire atmosphere, thereby providing an estimate of the total atmospheric seeing (ε_{TOT}). On the other hand MASS does not sense optical turbulence near the ground but reconstructs turbulence profiles at six altitudes ($h = 0.5, 1, 2, 4, 8,$ and 16 km) above the telescope (Tokovinin & Kornilov 2007). From such profiles the seeing that would be seen by an observer 500 m above the telescope to the top of the atmosphere is computed. MASS therefore provides an estimate of the free atmospheric seeing ($\varepsilon_{\text{FREE}}$). Ground layer seeing is calculated using the following formula (Skidmore et al. 2009):

$$\varepsilon_g = \frac{\varepsilon_{\text{TOT}} - \varepsilon_{\text{FREE}}}{|\varepsilon_{\text{TOT}} - \varepsilon_{\text{FREE}}|} \left| \varepsilon_{\text{TOT}}^{5/3} - \varepsilon_{\text{FREE}}^{5/3} \right|^{3/5} \quad (1)$$

Weather sensors were also placed on the CFHT tower, below the platform supporting the optical instrumentation, and their measurements are used throughout this study as reference for observed pressure, temperature, relative humidity, and wind at the summit of Maunakea. The anemometer is not placed at a standard meteorological weather tower height of 10 m; rather, it is closer to 6 m above the ground. A new location for a wind sensor, perhaps a SODAR (SONic Detection and Ranging), away from the turbulence induced by upstream observatories is being investigated. Data from the weather sensors have a sampling frequency of about 60 s. More on the MD instrumentation specifications can be found in Schöck et al. (2009) and Skidmore et al. (2009). The MD has collected data in real time since 2009 September and they are available at <http://mkwc.ifa.hawaii.edu/current/seeing/>. The MASS and DIMM



Figure 1. CFHT instrument tower, showing the setting for the DIMM and MASS instruments, mounted at the top and weather sensors mounted just below the optical instruments' platform (courtesy of Tom Benedict, CFHT).

Table 1. Mean and median values of DIMM and MASS seeing and estimated ground layer seeing.

Nightly average	Mean	Median
DIMM	0.70	0.65
MASS	0.45	0.35
Ground layer	0.47	0.50

instruments are set to operate under the following thresholds: relative humidity <85 per cent and wind speed <14 m s⁻¹ (~50 km h⁻¹). At time of writing the MD has operated for over 2400 nights since 2009 September. An analysis of these data in terms of their nightly average values, with some climatological context follows in the next section.

3 CLIMATOLOGY OF SEEING ON MAUNAKEA

The magnitudes of average and mean seeing derived separately from the DIMM and MASS instruments reflect the differences in the free and total atmospheric seeing, respectively, being made by these instruments (Kornilov et al. 2007, Table 1). The average seeing tends to be dominated by a few bad nights during which seeing values are very large. Meanwhile, seeing during good nights only goes as low as 0.25–0.3 arcsec, with many readings throughout the night. Thus, the median seeing is more representative of the quality of seeing at Maunakea and is commonly used in other studies (Skidmore et al. 2009; Vernin et al. 2011). On average, the ground layer turbulence, derived from the MASS and DIMM data, accounts for two-thirds to three-quarters of the total seeing, while free atmospheric turbulence

accounts for the remaining one quarter to one-third. However, these contributions can vary significantly on a daily basis depending on various factors. The fractions listed above are in agreement with those found during the TMT characterization campaign (Schöck et al. 2009). The MD data confirm that Maunakea is an optimal site for ground astronomy as most of the optical turbulence comes from within the shallow ground layer (Chun et al. 2009; Skidmore et al. 2009).

The distributions of DIMM and MASS seeing are skewed left, with median seeing being better than the mean (Fig. 2 and Table 1), a fortunate circumstance for astronomy at Maunakea. Looking at the seasonal distribution of the observations, the best time for quality seeing is during the summer months, when winds are generally light and upper level ridges drift through the area (Fig. 3). June and September show the largest number of nights with very good total seeing (< 0.6 arcsec) and nights with fewer events of high surface winds (Fig. 3a), while late summer (August and September) shows the best free atmospheric seeing (Fig. 3b), because of ridging and weak winds aloft.

During the winter season, the westerly jet stream increases in strength and moves closer to Hawaii, resulting in more weather disturbances from the north entering the subtropical Central Pacific area. Stronger jet stream winds are associated with fronts, stronger surface winds, wind shear aloft, and gravity waves, all of which produce turbulence at various levels in the atmosphere and reduce the potential for quality seeing.

A seasonal component is also evident in ground layer seeing but less so. Episodes of strong surface winds, responsible for most of the ground layer turbulence, are not rare during the summer season. Although the surface winds do not exhibit the same magnitude found during the winter seasons, deep easterlies associated with

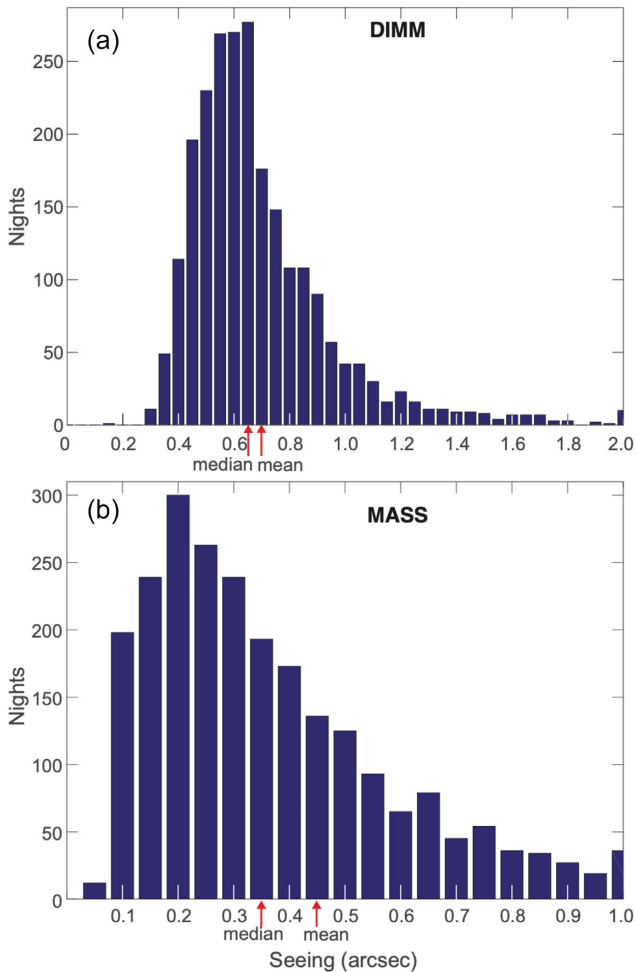


Figure 2. Distribution of the average nightly (a) DIMM and (b) MASS seeing, which reflect the differences in the free and total atmospheric seeing made by these instruments.

vertically stacked ridges or tight wind gradients between passing tropical disturbances to the south can result in episodes of stronger winds during the summer season, which can negatively impact seeing.

Time-series of MASS and DIMM data were created as follows: (i) nights when recording was either very short or very intermittent were eliminated from the sample; (ii) for each night only data falling in the 8 pm–4 am HST were retained to eliminate times of transition from day to night and vice versa; (iii) for each night, the average ground layer strength was also calculated; and (iv) a monthly rolling mean was applied to the nightly average DIMM, MASS, and ground layer seeing. The resulting time-series shows very good seeing dominating the record, with interannual and annual variability in the record (Fig. 4), and the end of 2014 stands out as a time of higher than average surface winds resulting in higher ground layer seeing. In contrast, the winter of 2018 shows elevated levels of free atmospheric seeing associated with the southward migration of a very strong jet stream aloft that brought significant wind shear over Maunakea.

The variability of seeing observations in Fig. 4 is quantified in the time-series in Fig. 5. In general, as the seeing degrades, the variability increases. From 2015 through 2016, the impact of the strong El Niño event can be seen in the good quality of seeing and reduced variability during this period (Kodama & Businger 1998).

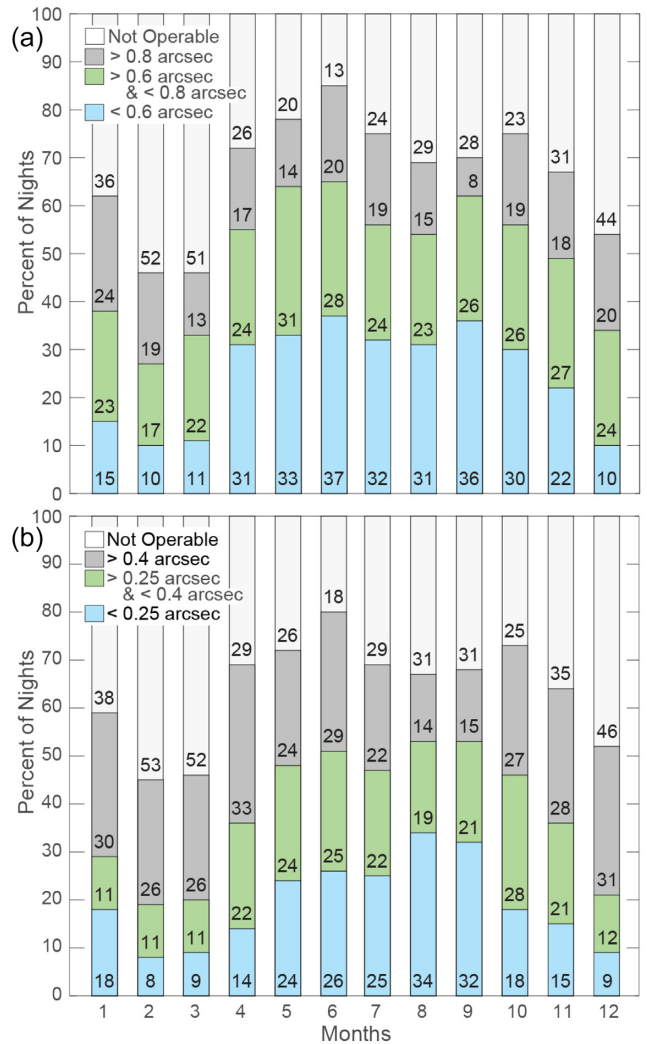


Figure 3. Monthly distributions of the nightly averaged seeing as measured by the (a) DIMM and (b) MASS accumulated since the instruments began operation. The numbers within the bars indicate the number of cases per year falling in that particular category.

Warm sea surface temperatures along the equator south of Hawaii during El Niño events cause a persistent ridge of high pressure to develop over Hawaii.

4 FORECASTING SEEING

The analysis that follows is intended to summarize forecaster experience in inferring relationships between synoptic patterns observed in the GFS (NCEP, <https://www.emc.ncep.noaa.gov>) analyses with the optical turbulence measures provided by the MASS and DIMM at the summit of Maunakea over almost a decade of data collection. The GFS model output provides 3D-grid analyses for standard operational meteorological fields. This study references the GFS pressure, wind, temperature, precipitable water, and relative humidity analysis fields. In forecasting seeing, the contributions from the ground layer and free atmospheric turbulence are considered separately, because they have distinct subgrid-scale sources that remain a challenge to quantify.

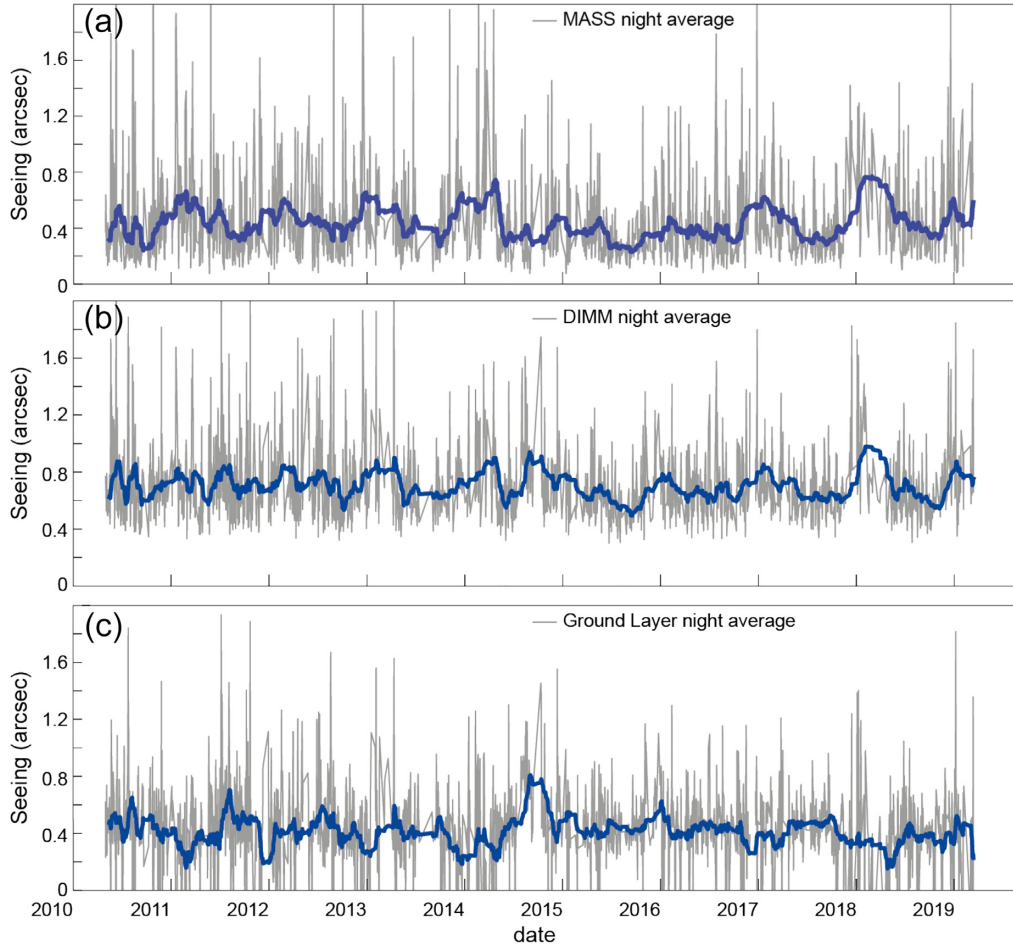


Figure 4. Time-series of measured seeing from 2010 May till present. Nightly 8-h average seeing measurements (grey lines) and their rolling monthly mean (blue lines), as measured from (a) DIMM, (b) MASS, and (c) as calculated for the ground layer.

4.1 Ground layer contribution

The GFS analyses and forecasts currently have a relatively low spatial resolution of 0.25° . In the past the model resolution was 0.5° , reduced from 1° previously, so there is an improving trend reflecting an increase in computational resources. Along with improved resolution, improved model physics and satellite data assimilation has resulted in a relatively accurate and consistent outlook in terms of average ground layer behaviour. This allows a preliminary diagnosis of the ground layer turbulence, which can be both dynamically and thermodynamically driven.

Generally speaking, there is a gradual increase in both mean and median seeing as winds begin to increase close to 5 m s^{-1} and this trend steepens at 7 m s^{-1} with mostly poor seeing prevailing once mean winds approach $8\text{--}9 \text{ m s}^{-1}$ (Fig. 6). This behaviour is consistent with that documented in Chun et al. (2009) and has often been observed while forecasting. A typical example of this behaviour is shown in Fig. 7. The DM measurements for this night indicate how total seeing (red dots) increases from an average $0.4\text{--}0.45$ arcsec during the beginning of the observing night to an average $0.7\text{--}0.8$ arcsec seeing as surface winds increase from ~ 7.5 to $\sim 10 \text{ m s}^{-1}$. The ground layer turbulence mechanically generated by the winds at the summit reaches the lowest level of the free atmosphere and spikes in the MASS measurements are noticeable in the lowest two layers, particularly the lowest layer centred at 500 m, from 11 pm

HST and through the rest of the night. As a result, the MASS seeing also shows an increase in time (blue dots in Fig. 7).

Less known and somewhat difficult to see in Fig. 6 is the slightly increasing trend in the mean and median seeing as wind decreases under very calm/dead winds. This behaviour is more evident in Fig. 8, which shows an increase in the seeing standard deviation as wind decreases. This increase is likely associated with bursts that result from unstable wave growth triggered by a shear-generated Kelvin–Helmholtz instability (Businger 1973, van der Linden et al. 2020). This instability generates turbulence that contributes to variability and/or degradation in seeing during relatively transient or prolonged periods of very weak winds. During the burst, the shear at the top of the ground layer is eroded and the initial cause of the instability is removed. Subsequently, the interfacial shear builds up again, causing the entire sequence to repeat itself with a time-scale of less than an hour. Fig. 9 shows an example of this behaviour. A spike in the total seeing recorded by the DIMM to $0.8\text{--}1.2$ arcsec corresponds to a period of dead wind ($\sim 0 \text{ m s}^{-1}$) during the second half of the night, while total seeing through the first part of the night showed an average of $0.4\text{--}0.5$ arcsec with winds ranging between $2\text{--}4 \text{ m s}^{-1}$.

Aside from wind, another variable that can affect optical turbulence is moisture. Usually the effect of moisture in the perturbation of the refractive index is not accounted for as, on average, only ~ 5 per cent of the atmosphere’s total water vapour lies above the summit. The moister air at lower elevations is capped well below

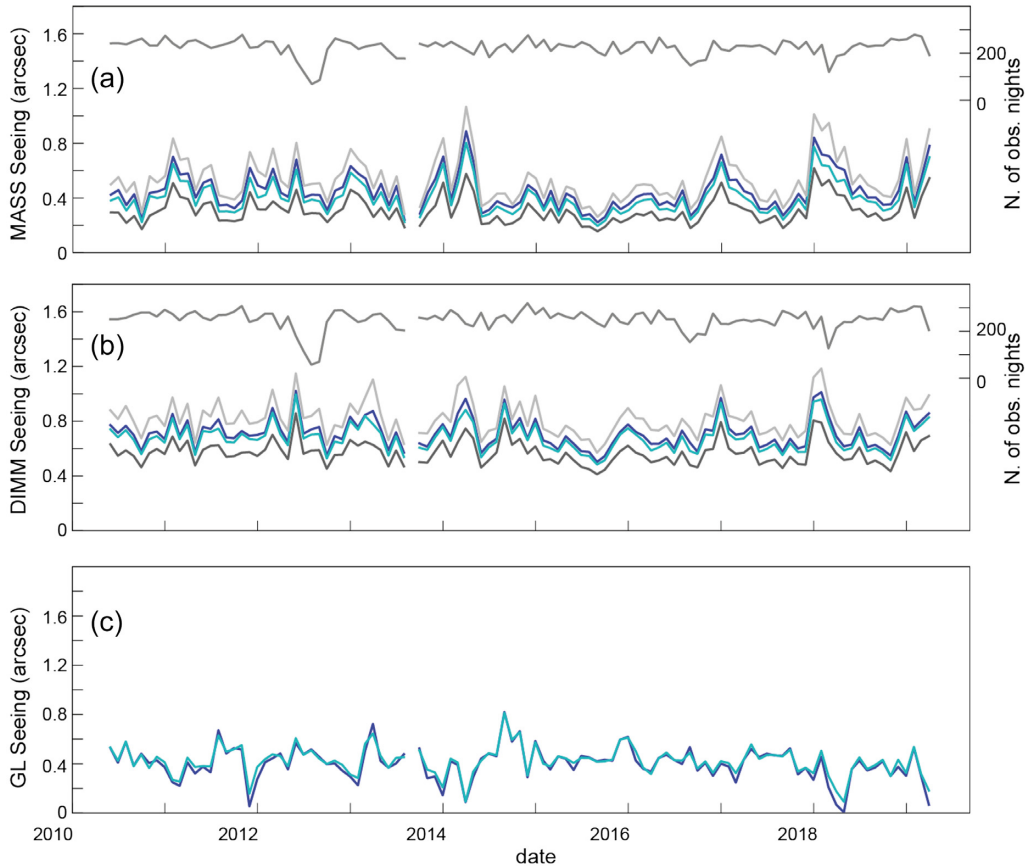


Figure 5. Time-series of monthly mean (blue line) and median (cyan line) for (a) DIMM, (b) MASS, and (c) ground layer seeing. For MASS and DIMM, the 25 per cent (dark grey) and 75 per cent (light grey) percentiles are also shown. Top solid light gray lines refer to the number of average monthly logged measures for both instruments (right y-axis).

the summit by strong, prevailing trade wind inversions. Thus, most of the telescope observing time is spent during very favourable, very dry, observing conditions. For astronomical purposes, it is therefore common practice to neglect the contribution from moisture in calculating the refractive index structure function C_n^2 and seeing.

However, there are instances where large variations and/or degradations of seeing occur because the trade wind inversion is elevated just below the summit. Under these conditions, winds or thermals can push pockets of moisture/clouds just beyond the inversion, where they detrain into the free atmosphere above the summit and evaporative cooling occurs, creating pockets of temperature and density gradients that contribute to fluctuations in seeing. A typical example of this phenomenon is depicted in Fig. 10(a), which occurs on average ~ 5 times per year, during otherwise good weather conditions when the MD is operating.

An example of an elevated trade wind inversion is shown in Fig. 10(b). The air mass over the summit was moist ($\text{RH} > 60$ per cent) during the day and first hours of the night and then began to dry, which allowed night operation. Nevertheless, spikes in relative humidity were recorded through the night, which was also reflected in temperature variations. Correspondingly, the observed DIMM seeing showed large variability and degradation, while the free atmosphere was relatively calm and the nightly average MASS seeing recorded was 0.15 arcsec.

While quantifying the effects of moisture and winds can be challenging, in general, winds greater than 6 m s^{-1} , prolonged

periods of calm winds, and/or an elevated trade wind inversion reaching just below the summit, are good indications of a large contribution from ground layer turbulence to total seeing, resulting in poorer than average seeing. Conversely, a very stable air mass with winds near $2\text{--}3 \text{ m s}^{-1}$ will generally contribute minimally to total seeing and allow for better than average seeing, although that will also depend on the contribution from the free atmosphere.

4.2 Free atmosphere contribution

In general, it is even more difficult to quantify free atmospheric turbulence than ground layer turbulence, mainly because of the small scale of the disturbances that traverse a range of elevations in the column above the summit. The ability to anticipate free atmospheric seeing is important because it provides guidance to the astronomy community in how best to utilize adaptive optics. It is quite rare (~ 16 per cent) for the free atmosphere on Maunakea to account for more than the mean total seeing (0.65 arcsec) and it only exceeds 0.5 arcsec about 25 per cent of the time. Consequently, under optimal summit-level conditions where the ground layer contribution to seeing is minimal, it is quite uncommon for poor to bad seeing to occur. Nevertheless, it is still necessary to use available resources to try and quantify the free atmosphere contribution to seeing, particularly during optimal summit-level conditions, and also to anticipate when poor/bad seeing is inevitable.

While predicting optical turbulence in general and, in the free atmosphere in particular, is a rather complex and non-linear problem,

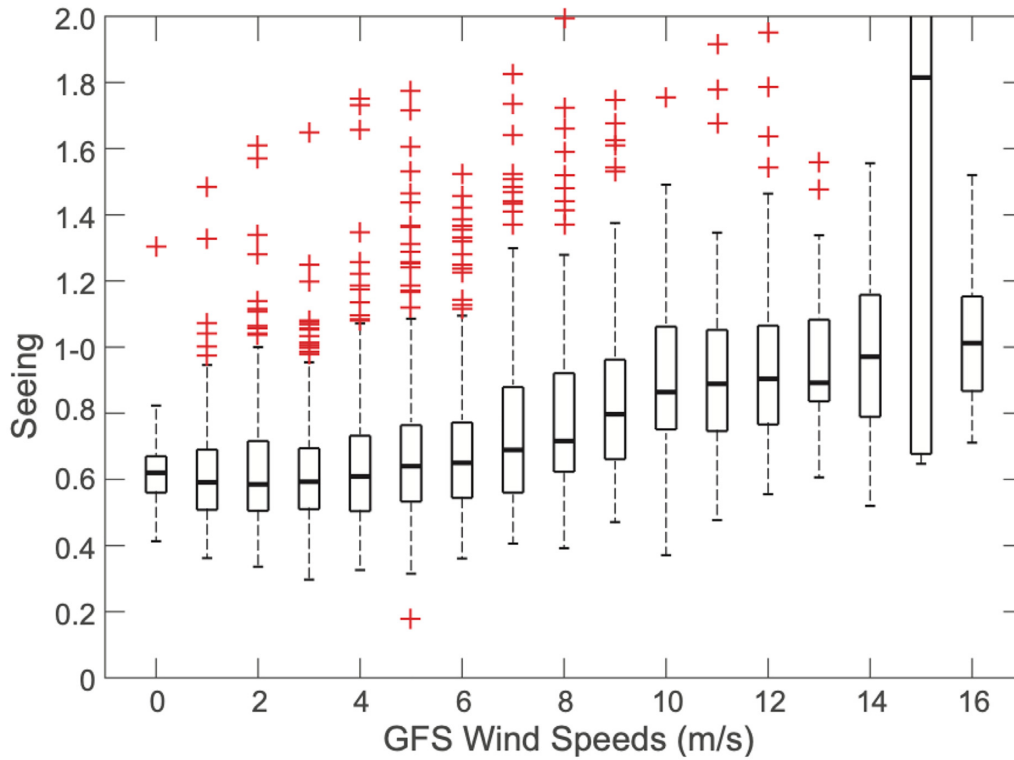


Figure 6. Nightly averaged DIMM measured seeing as a function of GFS surface winds from the model closest grid point to the MK summit location binned every 1 m s^{-1} . The box shows the median and extends from the 25 per cent to the 75 per cent percentiles of the data distribution. The whiskers indicate the data variability outside the upper and lower quartiles, while the red crosses indicate outliers.

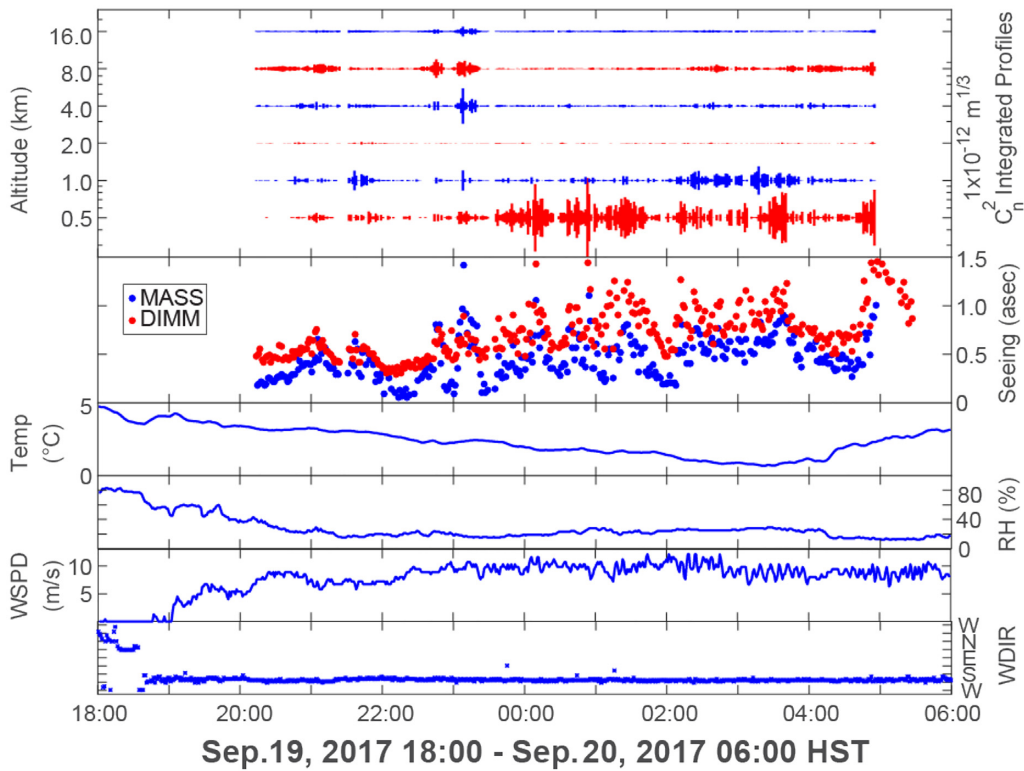


Figure 7. Summary of the observed conditions at the CFHT tower during the night of 2017 September 19–20. WSPD is the wind speed (m s^{-1}), WDIR is the wind direction (with WSENW indicating the rose wind directions), RH is the relative humidity (per cent), and Temp is the temperature ($^{\circ}\text{C}$).

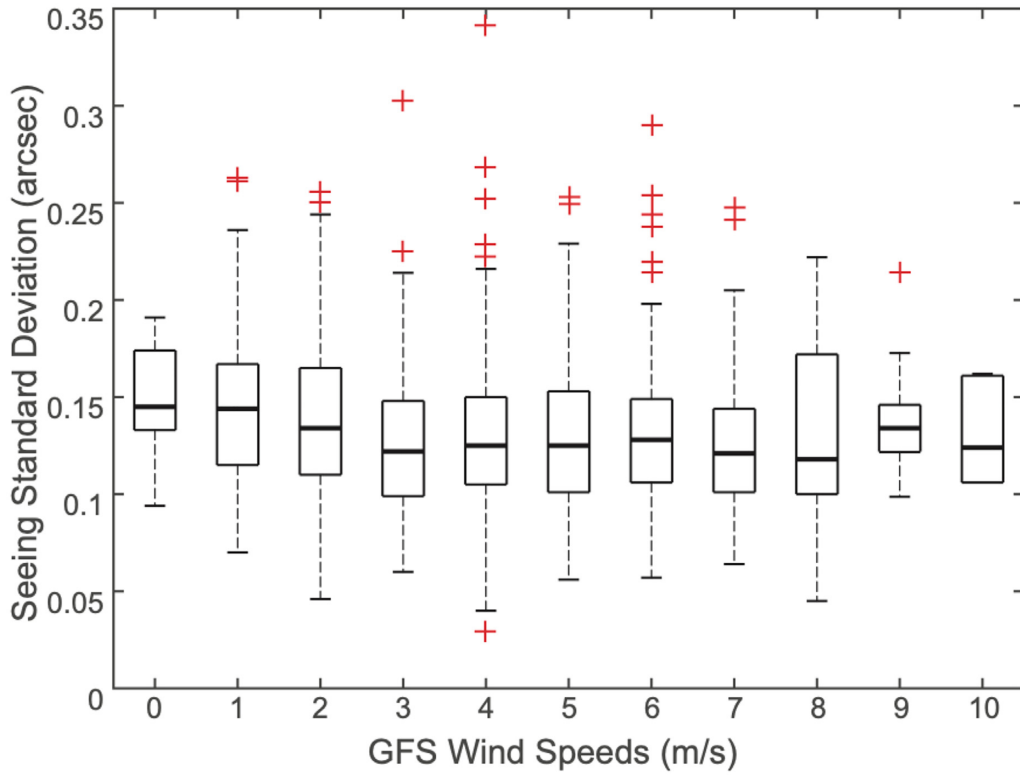


Figure 8. Seeing standard deviation as a function of GFS surface winds from the model closest grid point to the MK summit location binned every 1 m s^{-1} . As for Fig. 6, the box shows the median and extends from the 25 per cent to the 75 per cent percentiles of the data distribution. The whiskers indicate the data variability outside the upper and lower quartiles, while the red crosses indicate outliers.

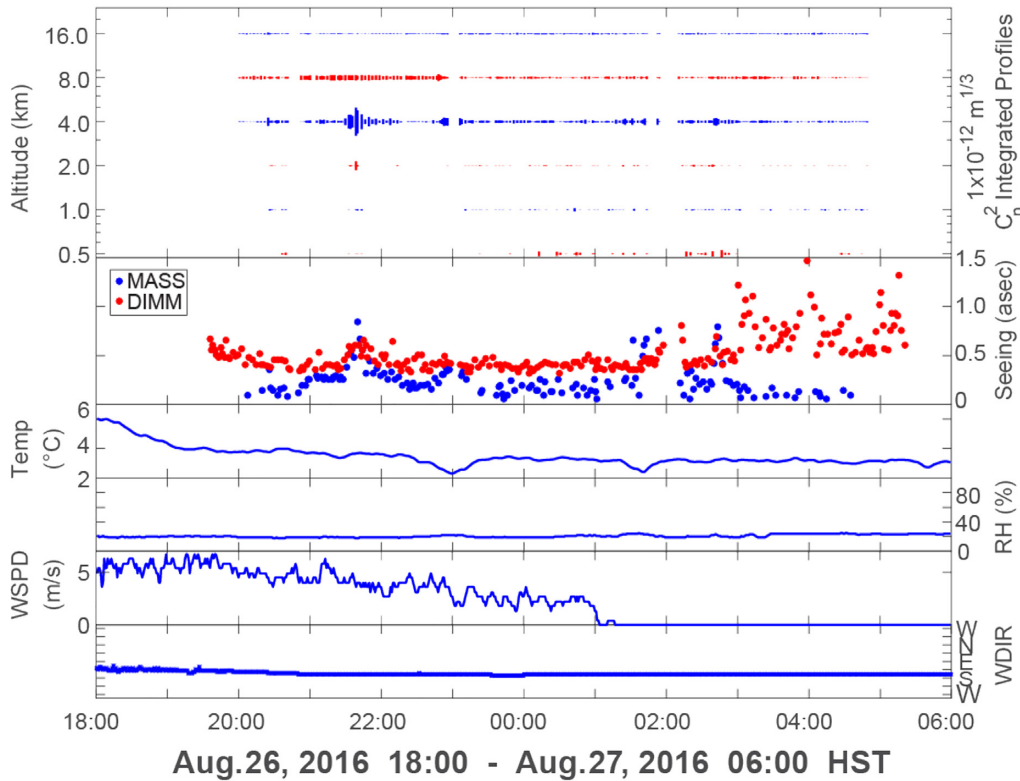


Figure 9. Summary of the observed conditions at the CFHT tower during the night of 2016 August 26–27. WSPD is the wind speed (m s^{-1}), WDIR is the wind direction (with WSEW indicating the rose wind directions), RH is the relative humidity (per cent), and Temp is the temperature ($^{\circ}\text{C}$).

Downloaded from https://academic.oup.com/mnras/article-abstract/496/4/4734/5865137 by guest on 29 July 2020

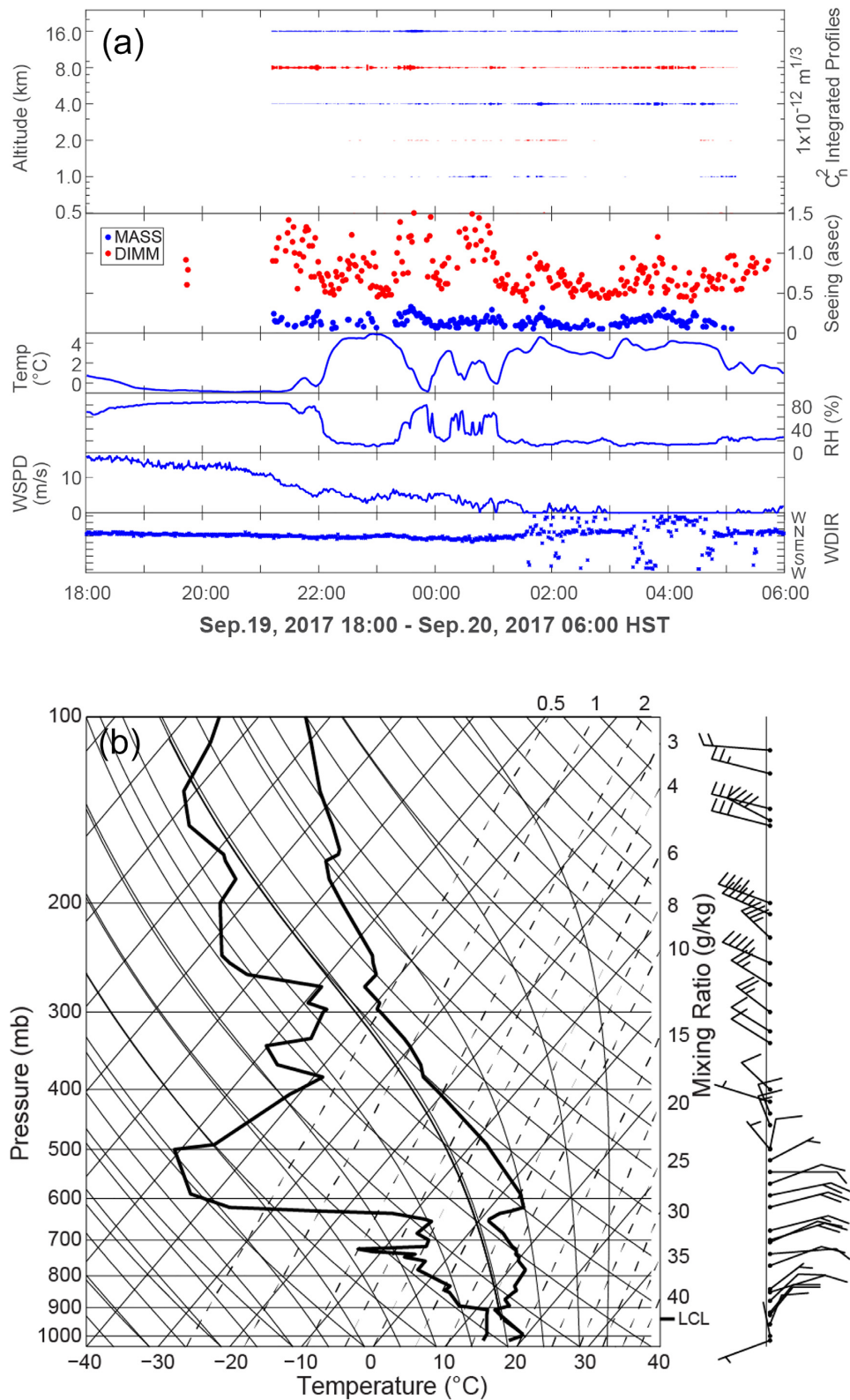


Figure 10. (a) Summary of the observed conditions at the CFHT tower during the night of 2017 March 19–20. WSPD is the wind speed (m s^{-1}), WDIR is the wind direction (with WSENW indicating the rose wind directions), RH is the relative humidity (per cent), and Temp is the temperature ($^{\circ}\text{C}$). (b) Hilo sounding at 12 UTC on 2017 March 20. The wind intensity and direction at various pressure levels is shown with barbs (<https://www.weather.gov/hfo/windbarbinfo> and <https://www.weather.gov/jetstream/skewt>).

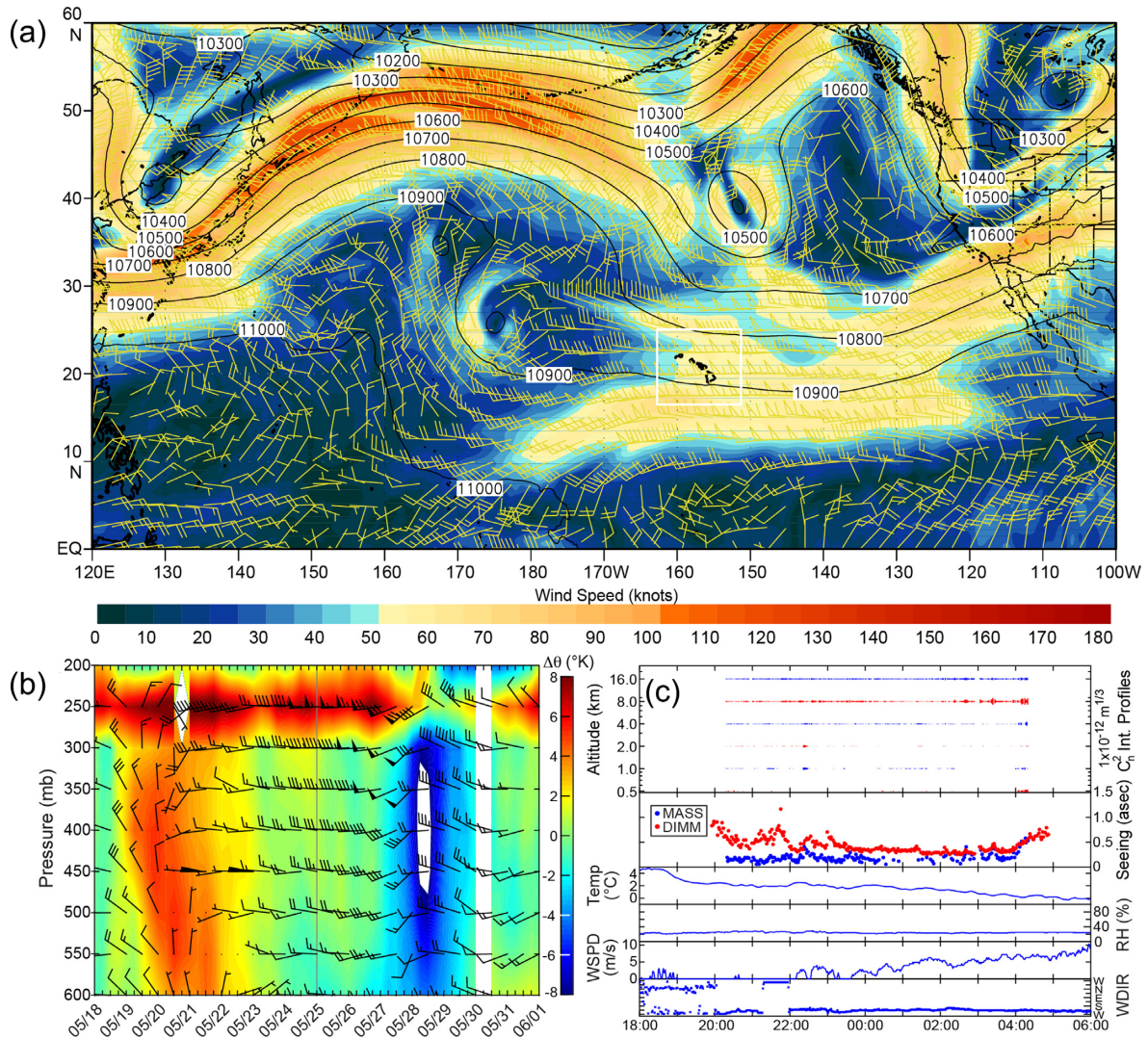


Figure 11. (a) The GFS analyses for wind (yellow barbs and colour shading) on 250 mb at 12UTC on 2017 May 25 showing a strong subtropical jet stream over the Hawaiian Islands and the Big Island. The location of the Hawaiian archipelago is indicated by a white box. Height contours (in metres) are also displayed; and (b) the GFS potential temperature and wind profile time-series leading to 2017 May 25. The vertical grey line indicates the date and time under discussion. The white areas denote missing data. (c) Summary of the observed conditions at the CFHT tower during the night of 2017 May 24–25.

the analysis of both the wind shear (vertical and horizontal) and changes in potential temperature with height through the atmosphere, can provide a good starting point. The following sections provide examples on how this works.

It would be tempting to assume that strong winds aloft, which are indicative of strong vertical wind shear, would generally translate to poor seeing: in reality, it is not that simple. Forecaster experience shows that, while sharp changes in wind direction and/or speeds with height in the free atmosphere could result in seeing degradation, their contribution rarely exceeds 0.5 arcsec. This is mainly because these abrupt changes occur near 10 km in the atmosphere and are associated with the subtropical or polar jet streams. At these higher altitudes the lower density helps to limit the magnitude of the optical turbulence. Moreover, during the winter when the jet stream shifts southward over Hawaii, its vertical extent (in pressure/altitude) can be rather large (order of 3–5 km). Within this layer, the winds can present a uniform/laminar flow regime that does not produce strong optical turbulence. Under these conditions, the free atmosphere contribution

to seeing can be minimal, and given light summit-level winds, better than average seeing can occur despite strong winds aloft.

Changes in potential temperature with height are a useful measure of the static stability of an unsaturated atmosphere. During stable periods, the potential temperature increases with height and vertical motions are suppressed. When the potential temperature decreases with height, the atmosphere is unstable and vertical motions occur. Both negative and positive changes in potential temperature, particularly sharp changes, are associated with degradations in seeing. Therefore, time-series plots of potential temperature with height are good diagnostic tools for the forecaster to use to diagnose the impact of changing stability in the troposphere on seeing.

Fig. 11(a) shows a strong subtropical jet stream over the Hawaiian Islands. Despite the strong upper level winds, the gradients of potential temperature are relatively small (Fig. 11b). The observed MASS seeing shown on Fig. 11(c) clearly depicts a calm free atmosphere, and an average nightly MASS seeing of 0.195 arcsec. Summit data confirm that the ground layer was quiet during the night

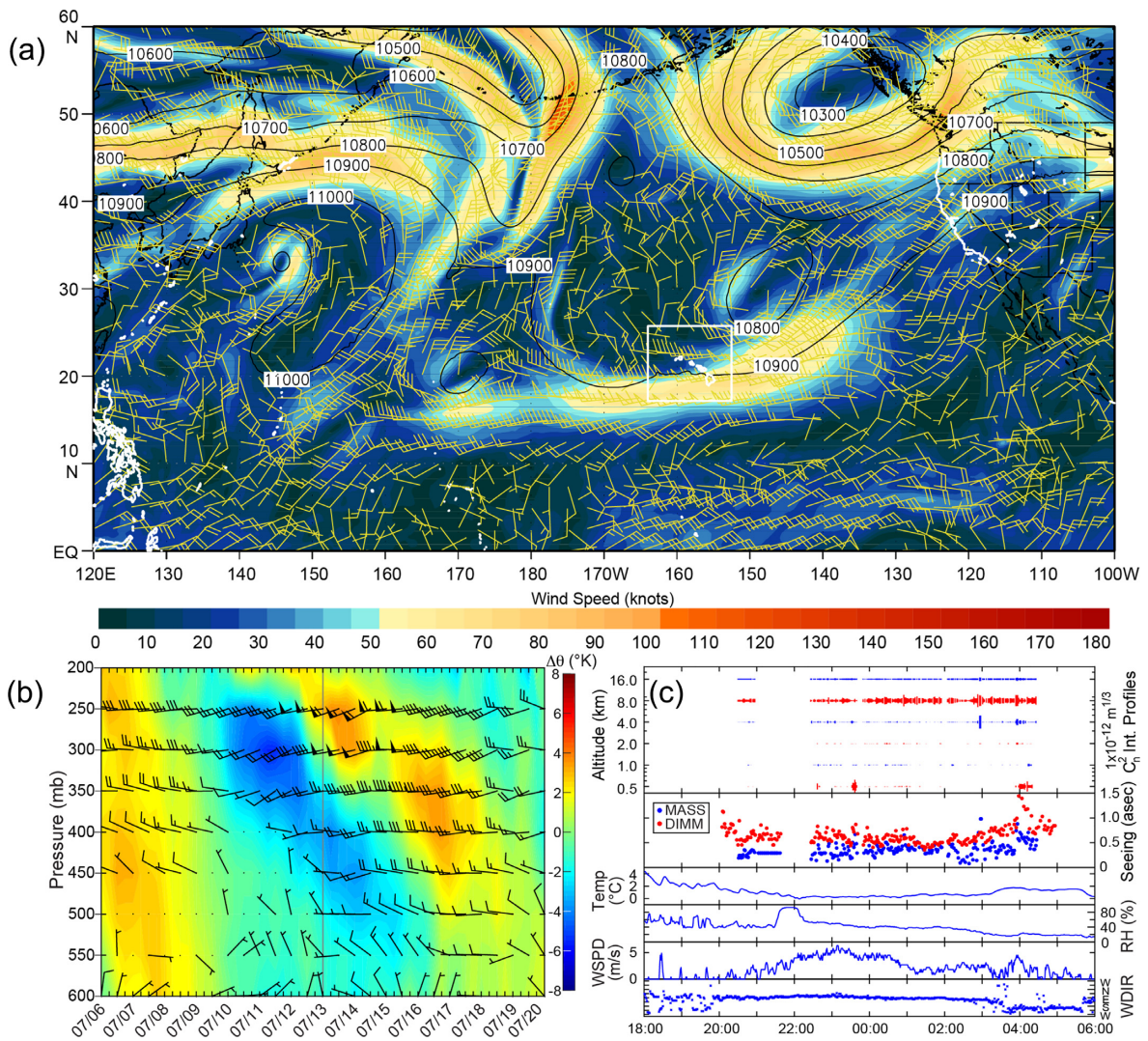


Figure 12. (a) The GFS analyses for wind (yellow barbs and colour shading) on 250 mb at 12UTC on 2017 July 13, showing a narrow subtropical jet stream over the Hawaiian Islands. The location of the Hawaiian archipelago is indicated by a white box. Height contours (in metres) are also displayed; and (b) the GFS potential temperature and wind profile time-series leading to 2017 July 13. The vertical grey line indicates the date and time under discussion. (c) Summary of the observed conditions at the CFHT tower on the night of 2017 July 12–13.

of the 2017 March 24 resulting in excellent seeing at the summit (Fig. 11c).

On occasions when the subtropical jet becomes very deep and strong, winds at the summit can increase significantly and the contribution from ground layer turbulence on total seeing becomes the limiting factor. Nevertheless, strong vertical wind shear ($> 25 \text{ m s}^{-1}$) occurs about 27 per cent of the time and can have a more prolonged effect on seeing although, again, its contribution is usually limited as discussed previously.

An example of strong vertical wind shear associated with a subtropical jet stream over Hawaii is shown in Fig. 12(a). In this case, the wind shear results in a contribution to MASS seeing from the upper levels, which in turn influences the total (DIMM) seeing (Fig 12c). However, its contribution to total seeing during this event averaged 0.36 arcsec, while mean seeing recorded by the DIMM is consistent with mean seeing for Maunakea.

Sharp horizontal wind gradients in the free atmosphere can produce turbulent eddies that can also disrupt seeing. While fairly well forecast by the GFS, it is difficult to anticipate the contribution to

seeing of this transient wind shear. These turbulent eddies are usually associated with the fringes of the subtropical or westerly jet streams, and tend to be short-lived (e.g. $< 3 \text{ h}$), and their contribution to seeing is small. Fig. 13 shows an example of horizontal wind shear impacting Hawaii on 2017 July 15 and 16, which contributed an average 0.26 arcsec to the total seeing. Nevertheless, the total seeing remained average to excellent through the night.

As mentioned previously, sharp changes in potential temperature are associated with degraded seeing. Time-series of potential temperature with height above the summit have proven useful in diagnosing cases in which the contribution to seeing from the free atmosphere equals the mean total seeing at the summit (0.65 arcsec). This is particularly true when rapid changes in potential temperature occur at heights below 4 km. For example, in Fig. 14 the potential temperature increased 6°C between 500–400 mb, which contributed to free atmospheric turbulence and a reduction in seeing, particularly during the early portion of the night. This event followed the passing of a front the night before, with a deep ridge producing strong static stability as it built into the area. In contrast, areas of instability in

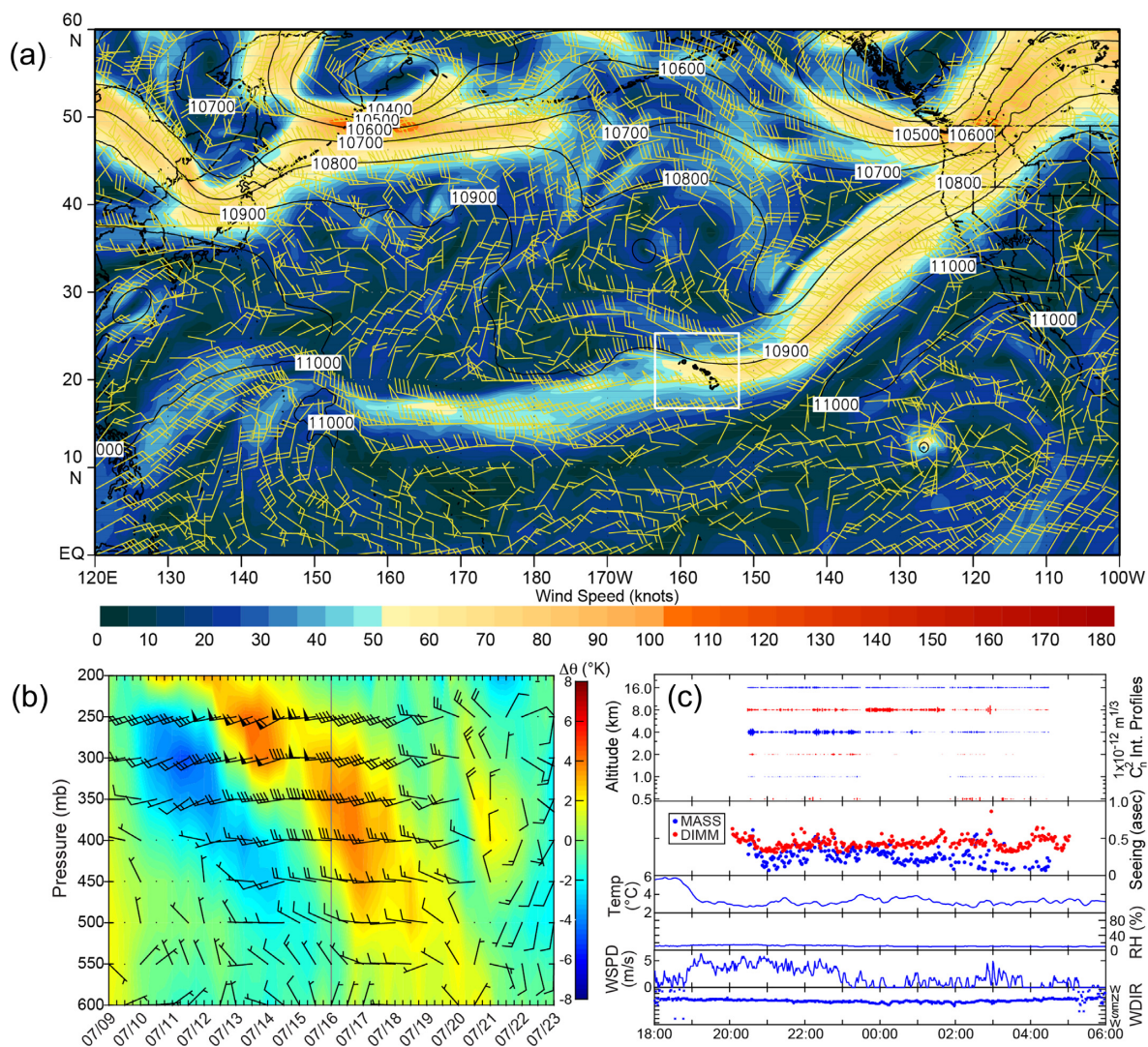


Figure 13. (a) The top panel shows the GFS analyses for wind (yellow bars and colour shading) on 250 mb at 12UTC on 2017 July 16, showing the fringes of a narrow/leaving subtropical jet stream over the Big Island. The location of the Hawaiian archipelago is indicated by a white box. Height contours (in metres) are also displayed; and (b) the GFS potential temperature and wind profile time-series leading to 2017 July 16. The vertical grey line indicates the date and time under discussion; and (c) summary of the observed conditions from the CFHT tower instrumentation, on the night of 2017 July 15–16.

the upper atmosphere and the impact of the optical turbulence at the tropopause represent small to negligible impacts on the total seeing, because of the significantly lower air densities at these levels.

4.3 Validation of seeing forecasts

The MKWC maintains a record of forecasts, which includes seeing forecasts. These forecasts are compared with observational data to track trends in the forecast accuracy. A summary of these statistics for seeing is presented in Fig. 15. As the quality of seeing decreases, the scatter in the comparison scatter plot increases considerably (Fig. 15a), contributing to a larger average rms of near 0.4 arcsec. When the comparison is limited to nights where the observed and forecast seeing are better than 1 arcsec, the standard deviation is reduced to ~ 0.24 arcsec (Fig. 15b). This average rms value has held remarkably steady since ~ 2012 . There are minor variations in this plot since 2012, which can be attributed to seasonal and intraseasonal influences, advances in model guidance, and experience. The striking improvement seen after 2010 occurred after the introduction and

regular use of the potential temperature profile. The histogram of the occurrence of forecasts errors is strongly skewed left (Fig. 15c), showing that small forecast errors far outpace larger forecast errors on days of good seeing. Looking at the cumulative curve, 50 per cent of the forecasts have errors less than 0.1 arcsec, 75 per cent of the forecasts have errors less than 0.24 arcsec, and 90 per cent of the forecasts have errors less than 0.38 arcsec.

5 CONCLUSIONS AND DISCUSSION

The range and quality of astronomical observations are greatly impacted by optical turbulence. Accurate forecasts of atmospheric optical turbulence provide important guidance that helps astronomers decide which instrument to schedule and enables them to optimize the adaptive optics technology that improves image resolution. Turbulent-scale perturbations can make the difference between an excellent night and a poor one. In this paper, the contributions to and challenges in accurately forecasting optical turbulence and seeing are presented. The relatively data sparse environment in

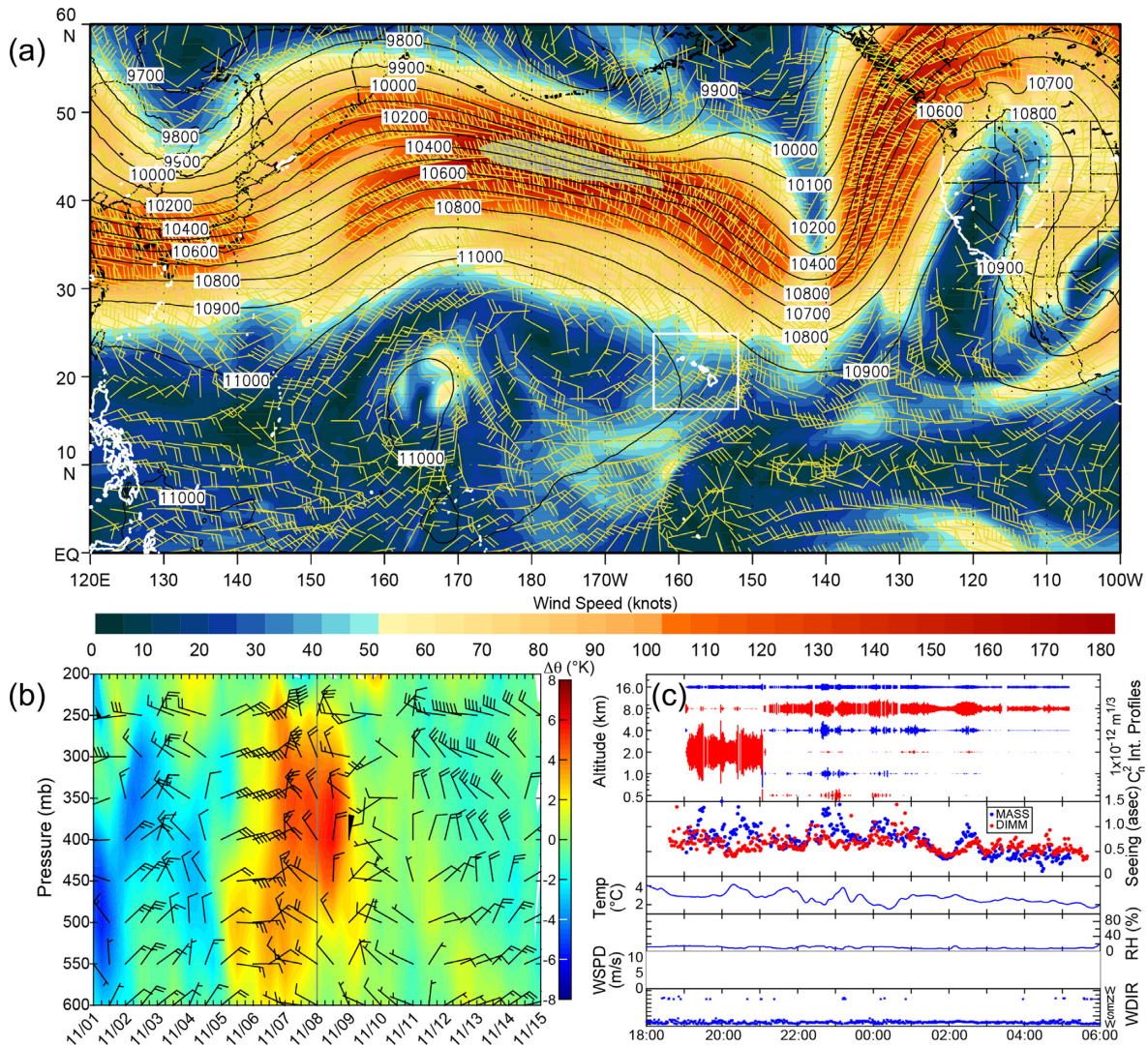


Figure 14. (a) The top panel shows the GFS analyses for wind (yellow bars and colour shading) on 250 mb at 12UTC on 2016 November 08. The location of the Hawaiian archipelago is indicated by a white box; height contours (in metres) are also displayed; and (b) the GFS potential temperature and wind profile time-series leading to 2016 November 08. The vertical grey line indicates the date and time under discussion. (c) Summary of the observed conditions at the CFHT tower during the night of 2016 November 7–8.

the Central Pacific compounds the overall challenge. Fortunately, the installation of reliable MASS and DIMM instrumentation on the summit of Maunakea has provided critical feedback during the past decade. The MASS and DIMM instruments provide a robust data set with which to investigate the variability in the quality of seeing in comparison to atmospheric conditions and seeing forecasts. The total seeing at the summit of Maunakea is comprised of contributions from mechanical turbulence in the ground layer and optical turbulence in the free atmosphere above. The following are a list of the conclusions supported by the data analysis in this research.

(i) The best seeing on average occurs during the summer months, when summit-level conditions are more favourable with lighter winds throughout the atmosphere and less risk of moisture and clouds over the summit.

(ii) August and September are months when the contribution from free atmospheric turbulence is lowest because of the more northerly position of a weaker summer jet stream and lighter winds aloft over Hawaii.

(iii) On average the contribution of ground layer turbulence is two-thirds to three-quarters of the total seeing, with free atmospheric turbulence contributing the remainder.

(iv) Summit winds of $2.5\text{--}5\text{ m s}^{-1}$ are associated with the smallest contributions to seeing from the ground layer.

(v) When summit winds are $< 2.5\text{ m s}^{-1}$, shear instability in the ground layer results in bursts of optical turbulence, resulting in intermittent poor seeing.

(vi) The summit seeing gradually deteriorates as winds increase above 5 m s^{-1} , with poor seeing and large variability in seeing occurring with summit winds $> 10\text{ m s}^{-1}$.

(vii) Low-level moisture infrequently reaches the summit, however, when it does the moisture gradients can play a role in degrading seeing by contributing rapid fluctuations in air density exacerbated by evaporative cooling. In general, summit moisture is accompanied by less stability in the atmosphere below the summit, often associated with the absence of or an elevated tradewind inversion.

(viii) When the ground layer turbulence is minimal, the free atmospheric turbulence accounts for two-thirds of the total seeing.

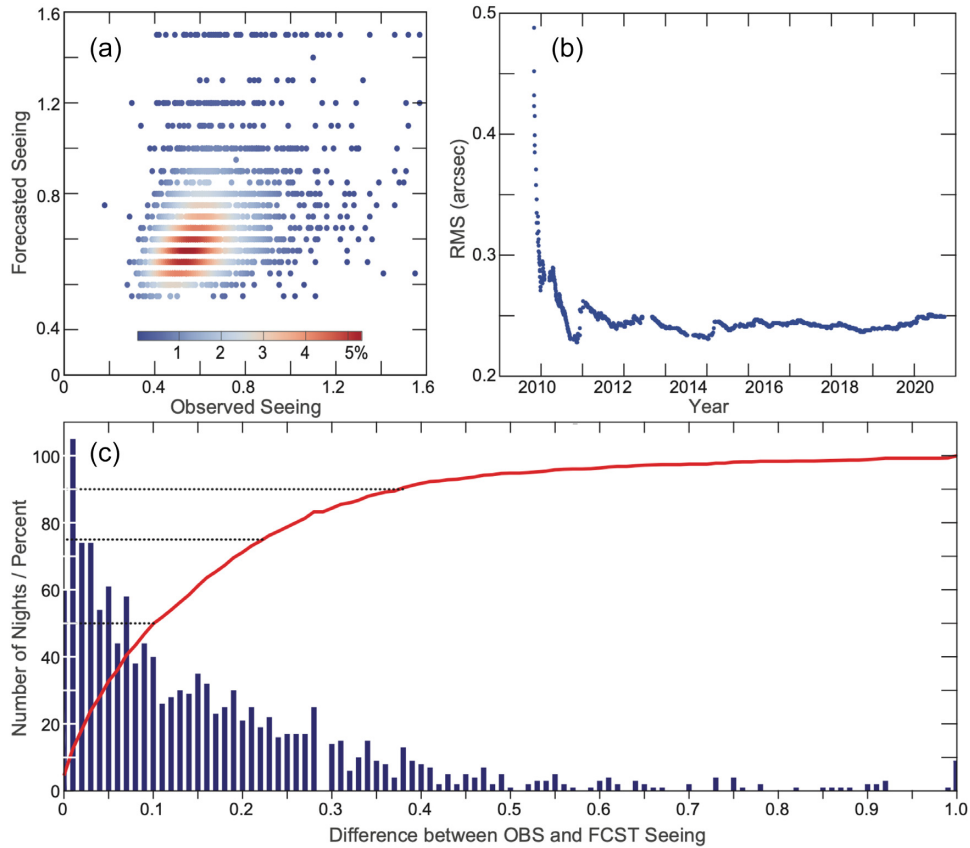


Figure 15. (a) Scatterplot of the observed versus forecast seeing for every night since 2009; the colour code represents the kernel density estimate for this data set. (b) Time-series of the forecast rms from 2009 to current for nights during which the observed seeing averaged less than 1 arcsec. (c) Distribution of the difference between observed and forecast seeing (blue histogram) and its cumulative curve (red line); the three dotted lines indicate the 50, 75, and 90 per cent thresholds, respectively.

(ix) For ~ 16 per cent of the nights, free atmospheric turbulence rarely exceeds 0.65 arcsec and for ~ 25 per cent of the nights it exceeds 0.5 arcsec.

(x) Contributions to free atmospheric turbulence include enhanced vertical and horizontal wind shear and enhanced vertical gradients in potential temperature (stability).

(xi) Enhanced horizontal wind shear is associated with the edges of jet streams and tends to be short lived.

(xii) Vertical wind shear is associated with sharp gradients in wind speed and/or direction and can have a more prolonged impact on the seeing.

(xiii) Sharp gradients in potential temperature with height significantly increase the potential for optical turbulence in the free atmosphere.

(xiv) Free atmospheric turbulence rarely exceeds the ground layer contribution to seeing.

(xv) Free atmospheric turbulence is challenging to forecast because it is associated with a combination of vertical and horizontal wind shear, and variations in static stability of the atmosphere.

(xvi) Rms errors in seeing forecasts for the summit of Maunakea have averaged < 0.25 arcsec since 2012, for good nights errors are < 1 arcsec. As the observed seeing becomes poorer, the rms forecast error also grows.

The analysis presented here outlines how forecasters have gained experience in anticipating the quality of seeing during the upcoming observing nights through daily forecasting activities. MKWC

forecasters begin by analysing large-scale meteorological features, such as the positions of the westerly and subtropical jet streams relative to the summit of Maunakea. Next, vertical gradients in potential temperature and vertical and horizontal wind shear aloft are analysed. Finally, the expected winds at the surface and the height of the trade wind inversion are diagnosed. Then, a combination of experience with local orographic influences and intuition are used to produce the MKWC predictions of both weather and optical turbulence parameters for the summit observatories.

It is common for a combination of changes in potential temperature, horizontal and vertical wind shear, and ground layer turbulence to make the seeing forecast very challenging. For these challenging circumstances, guidance from MKWC's high-resolution regional weather model is critical. Real time access to MASS and DIMM data has allowed for successful development of a customized algorithm that estimates seeing from model profiles (Cherubini & Businger 2013). The MKWC WRF model with the seeing algorithm is able to predict small-scale features and relate them to changes in the refractive index structure function C_n^2 , providing valuable guidance regarding the average nightly seeing. The output of the model system at hourly resolution enables forecasters to anticipate the temporal variability of seeing through the night.

The combination of modelling efforts and forecaster experience has resulted in improvements in seeing forecasts, with rms errors in seeing forecasts for the summit of Maunakea averaging < 0.25 arcsec since 2012, when poor weather conditions are excluded. An interesting opportunity that has resulted from the research in this

paper is the application of machine learning to the GFS variables that are found to be important in forecasting seeing. Further discussions of the application of WRF, seeing algorithms, and machine learning to foster additional improvements seeing forecasts will be the subjects of future papers.

ACKNOWLEDGEMENTS

Thanks go to the Maunakea Observatories for providing the MD database and to the CFHT staff for the operational support to the instruments and database, in particular to Marc Baril and Billy Mahoney. Thanks to Nancy Hulbert for her graphics support and to May Izumi for her editing of the final manuscript. We would like also to acknowledge high-performance computing support from Cheyenne (doi:10.5065/D6RX99HX) provided by the National Center for Atmospheric Research's Computational and Information Systems Laboratory, sponsored by the National Science Foundation. This research was supported by the National Science Foundation through the Maunakea Support Services, and the Office of Naval Research (ONR) under ONR award number N00014-18-1-2166.

DATA AVAILABILITY

The data underlying this article will be shared on reasonable request to the corresponding author.

REFERENCES

- Amico P., Campbell R.D., Christou J.C., 2010, *Proc. SPIEE*, 7737, 77370A
- Bougeault P., De Hui C., Fleury B., Laurent J., 1995, *Appl. Opt.* 34, 3481
- Businger S., McLaren R., Ogasawara R., Simons D., Wainscoat R.J., 2001, *Bull. Amer. Meteor. Soc.*, 83, 858
- Businger J. A., 1973, in Haugen D. A., ed., *Workshop on Micrometeorology, Turbulent transfer in the atmospheric surface layer*. Amer. Meteor. Soc., Boston, p. 67
- Businger S., Cherubini T., eds, 2011, *Seeing Clearly: The Impact of Atmospheric Turbulence on the Propagation of Extraterrestrial Radiation*. VWB Publishing, Texas
- Cherubini T., Businger S., Lyman R., Chun M., 2008a, *J. Appl. Meteorol. Climatol.*, 47, 1040
- Cherubini T., Businger S., Lyman R., 2008b, *J. Appl. Meteorol. Climatol.*, 47, 3033
- Cherubini T., Businger S., 2011, in Businger S., Cherubini T., eds, *Seeing Clearly: The Impact of Atmospheric Turbulence on the Propagation of Extraterrestrial Radiation*. VWB Publishing, Texas
- Cherubini T., Businger S., 2013, *J. Appl. Meteorol. Climatol.*, 52, 498
- Chun M. et al., 2009, *MNRAS*, 394, 1121
- Coulman C.E., 1985, *ARA&A*, 23, 19
- Da Silva S.C., 2012, MS thesis, Department of Meteorology, University of Hawaii at Mānoa, p. 110 Available at: <http://www.soest.hawaii.edu/MET/Faculty>
- Giordano C., Vernin J., Ramiò H.V., Muñoz-Tuñón C., Varela A.M., Trinquet H., 2013, *MNRAS*, 430, 3102
- Kodama R.K., Businger S., 1998, *Weather Forecast.*, 13, 523
- Kornilov V. et al., 2007, *MNRAS*, 382, 1268
- Kornilov V.M., 2016, *Exp. Astron.* 41, 223
- Masciadri E., Vernin J., Bougeault P., 1999, *A&AS*, 137, 185
- Masciadri E., Jabouille J.P., 2001, *A&A*, 376, 727
- Masciadri E., Avila R., Sánchez L., 2004, *Rev. Mex. Astron. Astrofis.*, 40, 3
- Masciadri E., Lascaux F., Fini L., 2013, *MNRAS*, 436, 1968
- Milli J. et al., 2019, preprint ([arXiv:1910.13767](https://arxiv.org/abs/1910.13767))
- Roddier F., 1981, *Prog. Opt.*, 19, 281
- Schöck M. et al., 2009, *PASP*, 121, 384
- Skidmore W. et al., 2009, *PASP*, 121, 1151
- Tokovinin A., 2002, *PASP*, 114, 1156
- Tokovinin A., Kornilov V. 2007, *MNRAS*, 381, 1179
- Trinquet H., Vernin J., 2009, Using meteorological forecasts to predict astronomical 'seeing', SPIENewsroom. Available at: <https://spie.org/news/1704-using-meteorological-forecasts-to-predict-astronomical-?SSO=1>
- Van Der Linden S.J.A., Van De Wiel B.J.H., Petenko I., Van Heerwaarden C.C., Bass P., Jonker H.J.J., 2020, *J. Atmos. Sci.*, in press
- Vernin J. et al., 2011, *PASP*, 123, 1334

This paper has been typeset from a Microsoft Word file prepared by the author.